Weak Plaquette Valence Bond Order in the S=1/2 Honeycomb J_{1}-J_{2} Heisenberg Model

Zhenyue Zhu, David A. Huse, and Steven R. White

Phys. Rev. Lett. **110**, 127205 — Published 18 March 2013

DOI: 10.1103/PhysRevLett.110.127205

Weak plaquette valence bond order in the $S = 1/2$ honeycomb $J_1 - J_2$ Heisenberg model

Zhenyue Zhu,[1] David A. Huse,[2] and Steven R. White[1]

[1]*Department of Physics and Astronomy, University of California, Irvine, CA 92697*
[2]*Department of Physics, Princeton University, Princeton, NJ 08544*

(Dated: February 13, 2013)

Using the density matrix renormalization group, we investigate the $S = 1/2$ Heisenberg model on the honeycomb lattice with first- (J_1) and second-neighbor (J_2) interactions. We are able to study long open cylinders with widths up to 12 lattice spacings. For J_2/J_1 near 0.3, we find an apparently paramagnetic phase, bordered by an antiferromagnetic phase for $J_2 \lesssim 0.26$ and by a valence bond crystal for $J_2 \gtrsim 0.36$. The longest correlation length that we find in this intermediate phase is for plaquette valence bond (PVB) order. This correlation length grows strongly with cylinder circumference, indicating either quantum criticality or weak PVB order.

PACS numbers: 75.10.Kt, 75.10.Jm, 73.43.Nq

Progress in finding realistic model quantum Hamiltonians with spin-liquid (SL) ground states has accelerated dramatically in the last two years, almost 40 years since Anderson first proposed a resonating valence bond (RVB) state as a possible ground state of the triangular Heisenberg model [1]. One key recent advance was the discovery using the density matrix renormalization group (DMRG) of a gapped SL ground state in the spin-1/2 kagome Heisenberg antiferromagnet [2, 3]. Spin liquid phases have been suggested for various other models, such as the half-filled honeycomb Fermi-Hubbard model [4] and the square lattice spin-1/2 Heisenberg antiferromagnet with second-neighbor (J_2) interactions [5, 6]. However, some skepticism has been expressed about the evidence for spin liquids in the latter two models [7, 8].

The main defining feature of a quantum spin liquid is the absence of any spontaneously broken symmetry, particularly either magnetic or valence-bond order. Frustration, which discourages order, is a key ingredient of models potentially containing spin liquid phases. Spin liquids arise in several analytic treatments and exactly solvable, simplified, but less realistic models [9]. A key feature distinguishing types of spin liquids is the presence or absence of a gap to all excitations. The kagome Heisenberg spin liquid is found to be gapped. To satisfy the Lieb-Schultz-Mattis theorem, gapped spin liquids for models with a net half-integer spin per unit cell must have "hidden" topological degeneracies in the thermodynamic limit, which depend on the topology of the system. The simplest possibility is a Z_2 spin liquid. Since local measurements cannot identify Z_2 or other topological orders, it is challenging to identify its presence in a numerical study. The degeneracies characteristic of a 2D gapped Z_2 spin liquid have not been accessible for the system sizes studied to date. Odd-width cylinders spontaneously dimerize in a pattern that is characteristic of a quasi-one-dimensional system [2, 5]. Another key feature of a Z_2 spin liquid is the presence of a $-\ln 2$ constant term correction to the linear growth of the entanglement entropy with subsystem perimeter. This term has now been measured in the nearest-neighbor kagome system [3] and also in the kagome system with next-nearest-neighbor interaction J_2 [10], where for $J_2 = 0.1$ the gaps are large and the entanglement entropy correction term can be measured particularly precisely. Thus, there is now solid evidence that the ground state of the kagome spin-1/2 antiferromagnet is a gapped Z_2 spin liquid.

In this paper, we examine the spin-1/2 Heisenberg antiferromagnet on the honeycomb lattice (see Fig. 1(a)) with Hamiltonian

$$H = J_1 \sum_{\langle i,j \rangle} S_i \cdot S_j + J_2 \sum_{\langle\langle i,j \rangle\rangle} S_i \cdot S_j \ . \qquad (1)$$

where the sum over $\langle i,j \rangle$ runs over nearest-neighbor pairs of sites and the sum $\langle\langle i,j \rangle\rangle$ runs over next-nearest-neighbors. We take $J_1 = 1$ (antiferromagnetic (AF)) and consider only $J_2 > 0$. Our work follows other studies of this and similar Heisenberg models [11–20], motivated by the Hubbard model results [21]. Most of these studies report a nonmagnetic phase near $J_2/J_1 \sim 0.2 - 0.4$, and we agree, but the results are in general disagreement on the range and nature of this phase. A variational Monte Carlo study indicated a spin liquid in the range 0.08 to 0.3 [20]. A combination of exact diagonalization and valence-bond treatment reported a plaquette valence bond (PVB, see Fig. 1(b)) crystal in the range 0.2-0.4 [11]. Exact diagonalization on small lattices [12], and the coupled-cluster method both suggest plaquette valence bond (PVB) order [13]. Earlier work reported that dimer correlations aren't strong enough for PVB order [16]. Functional renormalization group work claims this phase has weak dimer and plaquette response [15]. Variational entangled plaquette states suggest that none of the order parameters remain nonzero [19]. Other theoretical work has focused on the possibility of a Z_2 SL on the honeycomb lattice and on phase transitions between Neel and staggered valence-bond crystal (SVBC) phases [22–24].

Here we report that the ground state displays an apparently paramagnetic phase for $0.26 \lesssim J_2 \lesssim 0.36$. For

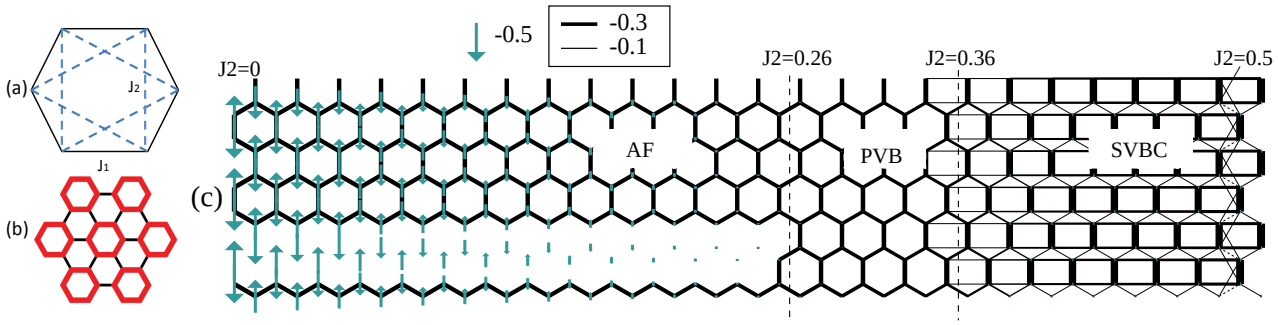

FIG. 1: (color online) (a) One hexagon of the honeycomb lattice showing J_1 and J_2 interactions. The six sides of the hexagon are J_1 bonds and the six J_2 bonds are shown as (blue) dashed lines. (b) Illustration of the pattern of plaquette valence bond (PVB) order. The spin-spin correlations differ between the bonds shown thin (black) vs. thick (red). (c)Three phases on the YC6-0 cylinder with 300 sites and a gradient of J_2. The widths of lines are proportional to $|\langle S_i \cdot S_j \rangle|$. We also show the second-neighbor spin correlation, but only when its value is negative. The arrows represents the values of $\langle S_i^z \rangle$ at each site. The scales for correlations and magnetizations are indicated. We remove several bonds in one zigzag row of the cylinder, so that the AF spin pattern is more clearly seen. The two vertical lines at $J_2 = 0.26$ and 0.36 indicate estimates of the phase boundaries.

$J_2 \lesssim 0.26$, we find the usual two-sublattice AF phase. For $J_2 \gtrsim 0.36$, we find a staggered valence bond crystal (SVBC). We have studied in some detail the system with $J_2 = 0.3$, deep within the intermediate phase that is neither AF nor SVBC. We examine various correlation functions of this ground state on various cylinders. The longest correlation length that we find is for PVB order. The strong growth of the PVB correlation length with cylinder circumference indicates that the system is either near a quantum critical point or may have weak long-range PVB order.

We use cylindrical (C) boundary conditions with open ends for our DMRG [25, 26] calculations. We label the cylinders either XCM-N or YCM-N. The labels X or Y indicated whether a first-neighbor bond is oriented horizontally (X) or vertically (Y). For XC cylinders, M is the number of sites along a zigzag vertical column and N means that the periodic boundary conditions are connected with a shift of N zigzag columns to the left or right. For YC cylinders, M is the number of zigzag horizontal rows and N means the connection has a shift by N sites along a zigzag row. For example, in the XC8-0 cylinder, one set of edges of each hexagon lie along the X direction, and there are 8 sites along the zigzag columns, which are connected periodically. So the circumference is $C = 4\sqrt{3}$ lattice spacings. For the YC4-0 cylinder, one set of edges of each hexagon lie along the Y direction and the cylinder is connected periodically along the Y direction with circumference 6 lattice spacings. For the XC9-1 cylinder, the connection has a horizontal shift of one zigzag column, producing a circumference of $C = 3\sqrt{7}$.

In Fig. 1(c), we present the ground state of a single system which gives an overview of the entire phase diagram. For this long YC6-0 cylinder, J_2 is uniform along the vertical direction, but varies linearly with the horizontal position from $J_2 = 0$ at the left edge to $J_2 = 0.5$ at the right edge. To make the AF order visible, we apply a staggered field at the left end of the cylinder. As J_2 increases along the cylinder, the AF order decreases, becoming negligible in the intermediate phase. We will discuss this intermediate state in detail below. The SVBC phase appears clearly for $J_2 \gtrsim 0.36$. This SVBC phase has strong first-neighbor correlations along the vertical direction with strong horizontal second-neighbor correlations connecting them to form "ladders". Below we will determine the phase boundaries of the AF and SVBC phases more accurately.

First we estimate the boundary of the AF phase. One technique to determine magnetic order parameters using DMRG is to put strong ordering fields on the edges of an open cylinder, and adjust the aspect ratio L_y/L_x to to minimize the finite size effects [27]. For both square and triangular spin-1/2 Heisenberg antiferromagnets, an aspect ratio near $1.7 \sim 1.9$ is found to minimize the finite size effects. For XCM-0 cylinders with M columns, the aspect ratio is $\sqrt{3}$, which we use. For $J_2 = 0$, we determine that $\langle S_z \rangle \cong 0.2720$, which is close to the value determined using Monte Carlo in the thermodynamic limit $\langle S_z \rangle = 0.2677(6)$ [28]. With J_2 increasing, we find that the magnetization reduces to near zero for $J_2 \cong 0.26$ in Fig. 2. The various cluster sizes all point to the phase transition near 0.26. This phase transition point is larger than the classical limit value of $J_2 = \frac{1}{6}$. Ref. [20] claims the Neel order disappears at 0.08, however the value we find here is more consistent with other studies which give $J_2 \cong 0.2$ [11, 14].

To estimate the boundary of the SVBC phase we study several XC cylinders with J_2 varying from 0.28 to 0.40 using the method in Fig. 1. These results show the SVBC phase for $J_2 \gtrsim 0.36$. We also use the entanglement entropy and its first derivative with respect to J_2 to estimate the phase transition point. We make vertical

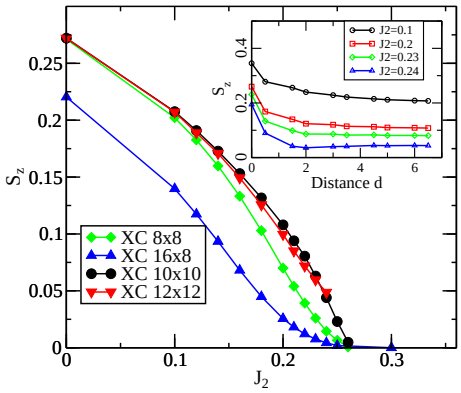

FIG. 2: (color online) The staggered magnetization at the center of the cylinder versus J_2 for various XC cylinders. The inset shows how the local magnetization decays from the edge of a long XC10 cylinder for various values of J_2.

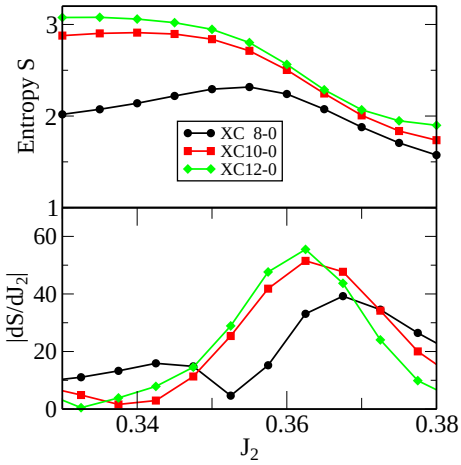

FIG. 3: (color online) The entanglement entropy and its derivative versus J_2 for different XC cylinders near the transition in to the SVBC phase.

cuts between zigzag columns, the dividing line between the two parts of the system bisecting a column of horizontal bonds, and measure the entanglement entropy. As seen in Fig. 3, the entropy drops in going from the intermediate phase to the SVBC. The derivative of the entropy shows a peak around 0.37 for the XC8-0 cylinder, and around 0.36 for the wider XC10-0 and XC12-0 cylinders. In addition, the height of this peak increases with the system width, as expected for a peak indicating a phase transition.[29–31]

On XC cylinders, we find the SVBC state has strong first- and second-neighbor correlations along diagonal directions, forming diagonally oriented ladders. Thus there are two degenerate diagonal SVBC states on an XC cylinder, whereas for YC cylinders there is only the one vertical SVBC pattern (Fig. 2). For an infinite two-dimensional system all 3 of these SVBC ground states would be degenerate by rotational symmetry. In the classical limit, for large J_2 values, the ground state is a spin spiral state. However, quantum fluctuations are strong enough to melt the spiral order and form the SVBC, in agreement with ref. [17].

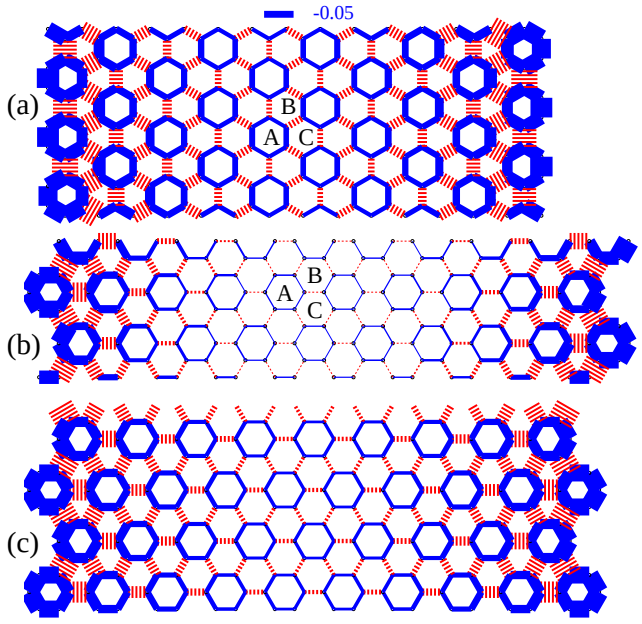

FIG. 4: (color online) Weak PVB order at $J_2 = 0.3$ on (a) YC7-3, (b) XC9-1 and (c) XC12-0 cylinders. The widths of the lines are proportional to $|\langle S_i \cdot S_j \rangle + 0.32|$ for all the plots, with blue solid(red dashed) lines for negative(positive) values. The bond strength scale is indicated at the top. The three different sublattices of plaquettes are labeled as A, B, C. In these figures we keep $m = 6000$ states in our DMRG calculation. The truncation error for XC9-1 is smaller than 10^{-7}, while it is near 10^{-6} for the wider YC7-3 and XC12-0 cylinders.

In the rest of this paper, we focus specifically on $J_2 = 0.3$ inside the intermediate phase [32]. To measure magnetic correlations, we apply "pinning" magnetic fields at one end of the cylinder, and measure the resulting magnetization pattern. Unlike in the AF phase, the induced magnetization decays exponentially from the end of the cylinder with a decay length of 2 to 3 lattice spacings for various cylinders. We further check the response to a local magnetic field applied to a spin at the cylinder center. This local magnetic field response is quite short ranged. It only influences its nearby surrounding sites, as opposed to generating a large region of staggered magnetization in the AF phase.

Refs. [11, 12] suggest that the intermediate phase is a PVB phase with long range dimer-dimer correlations. To investigate PVB ordering we study cylinders with periodic boundary conditions that are compatible with PVB order, including YC4-0, YC6-0, YC7-3, YC8-0, XC6-0, XC9-1 and XC12-0 [33]. We pin the PVB pattern at the cylinder ends by the choice of which spins are kept and

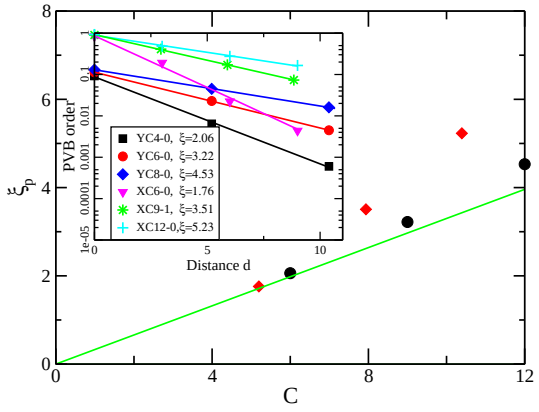

FIG. 5: (color online) PVB order correlation length ξ for different cylinder circumferences C at $J_2 = 0.3$. Black circles indicate YC cylinders; red diamonds indicate XC cylinders. The green straight line illustrates the expected linear behavior at the quantum critical point of the two-dimensional system. The inset shows the local PVB order parameter vs. distance from the end of the cylinder in lattice spacings. The estimated PVB correlation length ξ_p is indicated for each cylinder.

how long the cylinder is (see Fig. 4).

We define a local PVB order parameter at each site using the nearest-neighbor spin correlations on the 3 adjacent plaquettes. The plaquettes form 3 sublattices in the PVB phase, as labeled in Fig. 4 (a)-(b), and one plaquette from each sublattice is adjacent to each site. Let $E_A = -\sum_A \langle S_i \cdot S_j \rangle$ be the sum over the 6 bonds around plaquette A. Then we define the local PVB order parameter as

$$P = E_A + E_B \exp\left(\frac{2\pi}{3} i\right) + E_C \exp\left(\frac{4\pi}{3} i\right) . \qquad (2)$$

Near the ends of the cylinders, this order parameter is nonzero, and in general it is a complex number. We extrapolate this local order parameter versus the truncation error to estimate its values in the limit of large bond dimension m. For long cylinders, its magnitude decays exponentially with distance from the end, with a correlation length ξ_p that depends on the cylinder, as shown in the inset of Fig. 5. These PVB correlations can be slightly incommensurate, particularly for the narrower YC cylinders. For the XC9-1 cylinder with a shifted connection, we measure the distance from the end along the direction perpendicular to the wrapping vector, to obtain the shortest PVB correlation length ξ_p.

The PVB correlation length ξ_p versus cylinder circumference C is shown in Fig. 5. This figure includes cylinders with all orientations, and we see that for our larger circumferences, the XC cylinders appear to have a longer PVB correlation length than the YC cylinders. If the 2D system is at a quantum critical point, the correlation length is expected to be proportional to the circumference, by standard finite-size scaling. It appears that the correlation length actually increases faster than the circumference, suggesting that this system may have weak PVB long range order in the 2D limit of infinite circumference.

In conclusion, we have studied the $S = 1/2$ honeycomb $J_1 - J_2$ Heisenberg model on various cylinders extensively using DMRG. We find that the ground state displays a paramagnetic phase for $0.26 \lesssim J_2 \lesssim 0.36$. By studying PVB order on various cylinders, we find that the PVB correlation length grows at least linearly with the cylinder circumference. This suggests that in this phase the system is either quantum critical or has weak long-range PVB order. These results are compatible with an early theoretical study that a direct phase transition between an AFM and a PVB state, is possible on the honeycomb lattice [34].

We thank Hong-cheng Jiang, Miles Stoudenmire, Simeng Yan, Shoushu Gong, Olexei Motrunich, Donna Sheng and Tarun Grover for helpful discussion. We also like to thank A. M. Läuchli for providing their GS energy on a small torus. This work is supported by NSF grants DMR-0907500, DMR-1161348 and DMR-0819860.

Note added.—Recently we learned that Ganesh *et al.* [35] have studied the same model with DMRG. They reported that the ground state has three phases including Neel, f-wave PVB state and dimer state with critical points at $J_2/J_1 = 0.22$ and 0.35. Their findings are generally consistent with our results, and they also make the important point that this appears to be an example of deconfined quantum criticality.

[1] P. W. Anderson, Mater. Res. Bull. **8**, 153 (1973).
[2] S. Yan, D. A. Huse, and S. R. White, Science **332**, 1173 (2011).
[3] S. Depenbrock, I. P. McCulloch, and U. Schollwock, Phys. Rev. Lett. **109**, 067201 (2012).
[4] Z. Y. Meng, T. C. Lang, S. Wessel, F. F. Assaad and A. Muramatsu, Nature **464**, 847 (2010).
[5] H. C. Jiang, H. Yao and L. Balents, Phys. Rev. B 86, 024424 (2012).
[6] L. Wang, Z.-C. Gu, X.-G. Wen and F. Verstraete, arXiv:1112.3331 (unpublished).
[7] Sandro Sorella, Yuichi Otsuka, Seiji Yunoki, Scientific Reports **2**, 992 (2012).
[8] A. W. Sandvik, Phys. Rev. B **85**, 134407 (2012).
[9] L. Balents, Nature **464**, 199 (2010).
[10] H. C. Jiang, Z. Wang, and L. Balents, Nature Physics **8**, 902 (2012).
[11] A. F. Albuquerque, D. Schwandt, B. Hetényi, S. Capponi, M. Mambrini and A. M. Läuchli, Phys. Rev. B **84**, 024406 (2011).
[12] H. Mosadeq, F. Shahbazi, and S. A. Jafari, J. Phys.: Condens. Matter **23**, 226006 (2011).
[13] D. J. J. Farnell, R. F. Bishop, P. H. Y. Li, J. Richter and C. E. Campbell, Phys. Rev. B **84**, 012403 (2011).
[14] J. Oitmaa, and R. R. P. Singh, Phys. Rev. B **84**, 094424 (2011).
[15] J. Reuther, D. A. Abanin, and R. Thomale, Phys. Rev. B **84**, 014417 (2011).
[16] J. B. Fouet, P. Sindzingre, C. Lhuillier, Eur. Phys. J. B. **20**, 241 (2001).
[17] A. Mulder, R. Ganesh, L. Capriotti, and A. Paramekanti, Phys. Rev. B **81**, 214419 (2010).
[18] D. C. Cabra, C. A. Lamas, and H. D. Rosales, Mod. Phys. Lett. B **25**, 891 (2011).
[19] F. Mezzacapo and M. Boninsegni, Phys. Rev. B **85**, 060402 (2012).
[20] B. K. Clark, D. A. Abanin, and S. L. Sondhi, Phys. Rev. Lett. **107**, 087204 (2011).
[21] Note that the six spin interactions may be more important than the J_2 terms in properly characterizing the charge fluctuations in the Hubbard model [36, 37].
[22] F. Wang, Phys. Rev. B **82**, 024419 (2010).
[23] Y.-M. Lu and Y. Ran, Phys. Rev. B **84**, 024420 (2011).
[24] C. Xu and L. Balents, Phys. Rev. B **84**, 014402 (2011).
[25] S. R. White, Phys. Rev. Lett. **69**, 2863 (1992).
[26] S. R. White, Phys. Rev. B **48**, 10345 (1993).
[27] S. R. White, and A. L. Chernyshev, Phys. Rev. Lett. **99**, 127004 (2007).
[28] E. V. Castro, N. M. R. Peres, K. S. D. Beach, and A. W. Sandvik, Phys. Rev. B **73**, 054422 (2006).
[29] A. Osterloh, L. Amico, G. Falci, and R. Fazio, Nature **416**, 608 (2002).
[30] L.-A. Wu, M. S. Sarandy, and D. A. Lidar, Phys. Rev. Lett. **93**, 250404 (2004).
[31] O. Legeza and J. Solyom, Phys. Rev, Lett. **96**, 116401 (2006).
[32] The ground state energy per site, spin gaps are presented in section A of Supplemental Materials. And entropy analysis are presented in section C.
[33] We consider cylinders which don't accommodate PVB order, such as XC8-0 and XC10-0, in section B of Supplemental Materials.
[34] N. Read and Subir Sachdev, Phys. Rev. B **42**, 4568 (1990).
[35] R. Ganesh, J. van den Brink, and S. Nishimoto, arXiv:1301.0853 (unpublished).
[36] H.Y. Yang and K.P. Schmidt, Eur. Phys. Lett. **94**, 17004 (2011).
[37] H.-Y. Yang, A.F. Albuquerque, S. Capponi, A. Laeuchli, and K.P. Schmidt, New J. Phys. **14**, 115027 (2012).